
Article:
Reinke, M. L., Brunner, D., Golfinopoulos, T. et al. (10 more authors) (2019) Radiative heat exhaust in Alcator C-Mod I-mode plasmas. Nuclear Fusion. 046018. ISSN 1741-4326

https://doi.org/10.1088/1741-4326/ab04cf

Radiative Heat Exhaust in Alcator C-Mod I-Mode Plasmas

M.L. Reinke[1], D. Brunner[2], T. Golfinopoulos[2], A.E. Hubbard[2], J.W. Hughes[2], A.Q. Kuang[2], B. LaBombard[2], E. Marmar[2], R. Mumgaard[2], J.L. Terry[2], J. Lore[1], J. Canik[1], I. Cziegler[3], Alcator C-Mod Team

[1]Oak Ridge National Laboratory, Oak Ridge, TN 37831, USA
[2]Plasma Science and Fusion Center, Massachusetts Institute of Technology, Cambridge, MA 02139, USA
[3]York Plasma Institute, University of York, Heslington, York YO10 5DD, United Kingdom

E-mail: `reinkeml@ornl.gov`

DATE

Abstract. In order to more completely demonstrate the I-mode regime as a compelling fusion reactor operating scenario, the first dedicated attempts at I-mode radiative heat exhaust and detachment were carried out on Alcator C-Mod. Results conclusively show that within the parameter space explored, an I/L back-transition is triggered prior to meaningful reductions in parallel heat flux, $q_{\|}$, target temperature, $T_{e,tar}$ and target pressure, $p_{e,tar}$ at the outer divertor. The exact mechanism for the I/L trigger remains uncertain, but a multi-diagnostic investigation suggests the pedestal regulation physics is impacted promptly by small amounts of N_2 seeded into the private flux region. The time delay between when N_2 contacts the plasma and the I/L transition is triggered varied from 30-120 ms, approximately 0.7-3$\times\tau_E$, and the delay varied inversely with I-mode pedestal-top pressure, $p_{e,95}$. Power and nitrogen influx scans indicate that the I/L transitions are not linked to excessive bulk-plasma impurity radiation. It is also shown that in the subsequent L-mode following nitrogen seeding, $q_{\|}$ and $T_{e,tar}$ can be reduced by factors of $\simeq$10. The I/L transition and L-mode exhaust results using N_2 are compared to similar attempts using Ne where such $q_{\|}$ and $T_{e,tar}$ reductions in L-mode are limited to factors of 2-3. Implications for the I-mode regime are discussed, including needs for follow-up experiments on other facilities.

Keywords: power exhaust, divertor, impurity, I-mode, Alcator C-Mod, tokamak

Submitted to: *Nucl. Fusion*

1. Introduction

Confinement regimes have been studied in detail for their core-transport and pedestal properties, allowing empirical and physics-based extrapolations to larger machines

like ITER to ensure they support a net-generation of power. Less well established are credible power exhaust and particle control solutions, in which heat exhaust is manageable and erosion is effectively eliminated to increase lifetime of plasma facing surfaces. While this evolution has occured over decades for H-mode [1], the I-mode regime has only recently been explored and exhaust scenarios have not yet been demonstrated. While a regime with L-mode like particle and increased energy confinement regime was first observed on ASDEX Upgrade [2], in-depth investigation more recently has been motivated by Alcator C-Mod results [3]. I-mode has been further established on DIII-D [4] and AUG [5][6], while C-Mod has demonstrated a route to reactor relevant τ_E, in which higher field [7] enlarges the window in input power between the L/I transition and the I/H. Recently, the I-mode regime was extended to 8 T on C-Mod [8].

Power exhaust has been known to be an issue over multiple years of C-Mod I-mode studies. Low-density, high-power operation often resulted in elevating the steady-state Mo concentration originating from C-Mod's high-Z divertor and limiter plasma facing components PFCs. Injections of W from the melting of non-flush mounted Langmuir probes in the divertor were also not uncommon. In these cases small amounts of Ne would be used, tuned empirically to avoid high-Z impurity radiation from negatively impacting confinement. Some of C-Mod's most widely referenced I-modes, such as 1120907028 in [7], feature this trace level of Ne, indicating that moderate reduction of heat flux could be achieved through impurity seeding. But to more fully assess the I-mode regime as a scenario that can be used in long-pulse, reactor-scale devices, it is necessary to run dedicated experiments to further reduce the heat exhaust and operate I-mode in the detached divertor regime.

Alcator C-Mod results, utilizing low-Z (N_2, Ne) impurity seeding and a conventional vertical-plate, single-null divertor geometry, show that I-mode plasmas go through an I/L back-transition prior to exhibiting a meaningful reduction in any power exhaust and erosion control metrics required in the context of approaching detachment. The $q_{\|}$ and T_e at the outer target cannot be reduced more than 50% while keeping the thermal edge transport barrier (ETB) when seeding with either Ne or N_2. When using N_2 injected into the private flux region, there is a prompt drop instead of gradual decay in pedestal temperature indicative of a back-transition bifurcation from I-mode to L-mode. This stands in contrast to low-Z seeding scenarios in EDA and ELMy H-mode on C-Mod where as the seeding level is increased, the power into the pedestal is continually decreased and the H-mode is still sustained for $P/P_{LH} < 1$, although at reduced H_{98} [9][10].

The setup and operation of the I-mode radiative exhaust and detachment attempts are summarized in more detail in Section 2, alongside a description of key diagnostics. Experiments were done over two run days, composing approximately 50 detachment attempts which included I-mode targets at two different B_T and I_P combinations at fixed q_{95} and nominally fixed plasma shape, while conducting shot-to-shot variations in input power, and amount and type of impurity seeding. These experiments demonstrate

the limited ability to inject impurities while maintaining I-Mode, and that extrinsic seeding is indeed the cause of the change in confinement mode. A more detailed look at the ordering of events following the injection of the low-Z gas is presented in Section 3. Here it is shown that I-modes with the highest pedestal pressures and longest confinement time are those that are most susceptible to transitioning back to L-mode. A detailed investigation reveals that an initial response to seeding is a change in low frequency, 10-20 kHz, coherent oscillations as well as an increase in mid-frequency, 100's of kHz, density fluctuations, both estimated to be localized to near the top of the temperature pedestal. These point to an as yet unidentified mechanism whereby the low-Z seeding, in particular with N_2 into the private flux region (PFR), is interacting with the turbulence regulation mechanism(s) thought to be responsible for sustaining the edge thermal transport barrier. Despite the transition back to L-mode, there is still a substantial reduction, nearly a factor of 10, in outer target $q_{\parallel}$, T_e, as summarized in Section 4. This suggests the low-density, high temperature SOL plasma can still support significant dissipation, alluding to the possibility of future I-mode detachment scenarios that, through physics or engineering advances, mitigate edge transport barrier degradation while enhancing dissipation on open field lines. This is discussed in Section 5 along with other implications from these C-Mod experiments.

2. Description of Experiments

These I-mode experiments were conducted using the compact, high-field Alcator C-Mod tokamak [11]. Experiments were completed at 5.4-5.7 T using three antennas in the ion cyclotron range of frequency (ICRF) (78-80 MHz), employing the D(H) minority heating scheme that deposits power on-axis. Nitrogen was introduced using a divertor piezo system described in more detail in [12] in feed-forward mode which fuels into the low-field side private flux region. Neon was introduced using main chamber gas injection. As outlined in [3], the most robust I-modes are obtained by operating in a single null configuration with the $B \times \nabla B$ drift direction away from the active x-point. This was done on C-Mod by reversing both current and field allowing I-mode studies to take advantage of the closed, vertical plate divertor and its comprehensive set of diagnostics. This includes an array of toroidally extended 'rail-probes' [13], surface thermocouples (STC) [14] and multi-chord visible spectroscopy. Figure 1 shows the fields of view of the spectroscopy, where N II and Mo I time histories, discussed in Section 4 are averaged over multiple lines of sight. This also shows where the divertor pressure is measured, discussed below, and how the nitrogen is introduced into the PFR. Unfortunately, no multi-channel resistive bolometry is available during these experiments and the radiation is characterized using a wide-angle, so-called 2π bolometer which includes both core and divertor radiation. It is normalized empirically such that plasmas approaching radiative collapse from excessive high-Z radiation are defined to be 100% of the input power. Such a signal can only give an approximate picture of the radiated power. While it is sensitive to an increase in divertor radiation,

it will underreport the total radiated power if it includes a strong boundary radiator, but will be conservative estimate of the power crossing the separatrix, P_{SEP}, based on prior work with more comprehensive measurements[9]. Standard core diagnostics are used including pedestal Thomson scattering, interferometry, electron cyclotron emission (ECE) [15] as well as VUV spectroscopy [16]. The VUV spectroscopy measures radially along the midplane and thus does not represent local enhancement that may occure in the divertor. A reflectometer [17], gas-puff imaging [18] and AXUV and SXR diodes [19] are used to explore the fast pedestal/edge response.

An initial set of experiments scanned combinations and amounts of extrinsic impurities in 1.1 MA, $\bar{n}_e \simeq 1.5 \times 10^{20}$ m^{-3} plasmas with 4.0-4.5 MW of total input power (Ohmic and assuming 90% absorption of P_{ICRF}). The on-axis field in these shots was 5.7 T. A 2 Hz, 2-4 cm sweep in the inner and outer strike points was used to drop the time averaged heat flux as well increase the resolution of divertor diagnostics. ICRF heating was applied from $0.6 < t < 1.5$ seconds, causing a prompt L/I transition which reaches stationary conditions just before $t = 0.8$ seconds. Combinations were tested using a recycling impurity, injected into the main-chamber prior to establishing the I-mode, and a non-recycling impurity, injected into the PFR during the I-mode starting after $t \simeq 0.8$ s. Figure 2 shows a very brief overview of a three shot scan where the recycling gas is neon and the non-recycling gas is nitrogen. The recycling Ne required only an 80 ms puff, approximately 0.15 Torr-L, injected prior to the ICRF power turning on, to keep a quasi-stationary level in the plasma. At the highest level of N_2 seeding shown in Figure 2, $\simeq$9 Torr-L of nitrogen was injected over $0.7 < t < 1.40$ seconds. The response of the core plasma is represented by the time history of H_{98}, while the changes in the divertor were tracked through the target heat flux measured by time varying STC signals. Note the strike point sweep and dynamic evolution of the heat flux complicates this, so the location of the outer strike point, in units of the STC channel is also plotted. The largest levels of N_2 influx (black, blue traces in Figure 2), reflected by the strongest N VII emission seen in the core, show the strongest reduction in heat flux, but only following the reduction in confinement at $t \simeq 0.85$ s, corresponding to the I/L back-transition. Reducing the pressure in the N_2 seeding pleum by 86% (red traces in Figure 2) results in a slower, but eventual reduction of confinement back to L-mode, but corresponds to insufficient nitrogen to make meaningful impact on the heat flux. Both Ne and Ar were used as the initial recycling gas and varied in level from zero, in which case intrinsic Mo prevented I-mode from being established, up to levels where the recycling gas itself resulted in too much radiated power and also suppressed I-mode. In general, impurity seeding is not a requirement for establishing I-mode, as shown below, but at high P_{RF}/n_e it can aid in reducing intrinsic Mo, which increases P_{SEP}. For nitrogen, a slower response, more axisymmetric capillary system was also tried, as this system had been used successfully in recent H-mode detachment studies [20][21], but I-mode results were qualitatively similar to those using the divertor piezo injection. Over all scans with combinations of impurity gases and fueling methods, approximately 25 pulses, results were clearly limited to mitigating heat flux only in the

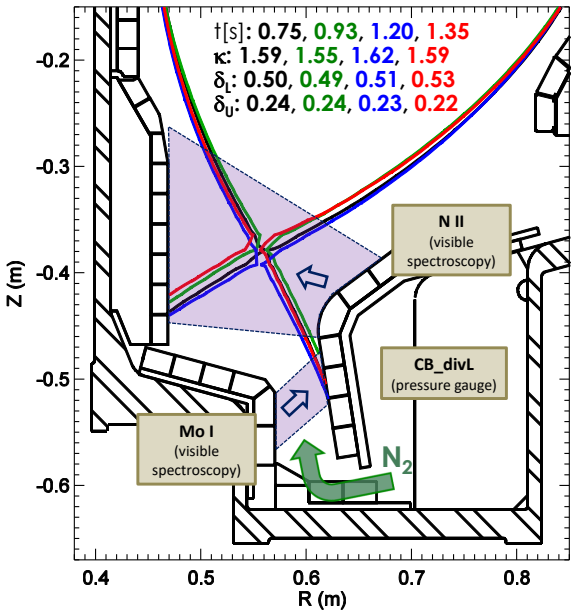

Figure 1: Partial layout of the divertor diagnostics relative to the sweeping equilibrium used and the N_2 seeding location. See [13] and [14] for details of the sensors embedded in the outer divertor.

L-mode phase, as shown in Figure 2.

Of particular importance is demonstrating that this phenomenology was indeed due to the impurity seeding. Because of the high input power, an I-mode plasma sustained for 0.8-1.0 seconds without seeding resulted in elevated Mo, degrading the pedestal by reducing net power feeding the edge transport barrier. Rather than compare seeded and unseeded plasmas, the causality of the effect of seeding was confirmed by moving the start time of the N_2 injection ahead by 150 ms in the I-mode flat-top, as shown in Figures 3 and 4. This comes from a set experiments which followed those illustrated in Figure 2, and were run at 1.0 MA and 5.4 T, but also at $q_{95} = 3.5$. No recycling impurity was used and lower input power avoided a problem with intrinsic molybdenum prior to seeding in most shots. All subsequent results discussed are from this I_p and B_T combination. The plots show transition dynamics are replicated at the earlier time, giving a strong indication that the impurity seeding is causing the back-transition and not a systematic error or coincidence. Despite large changes in the temperature that move with the puff timing, there is no indication of the confinement transition causing a change in the line-averaged density, shown in Figure 3, as expected for an I/L transition. Although not shown here, these plasmas show the same behavior discussed earlier where the back-transition precedes significant reductions in outer target heat load. Further details of the divertor response are outlined in Section 4.

A more detailed examination of the back-transition is shown in Figure 4. The pressure measurement in the space between the outer divertor plates and the vacuum vessel indicates the time at which the gas arrives in the torus, and soon after a slower

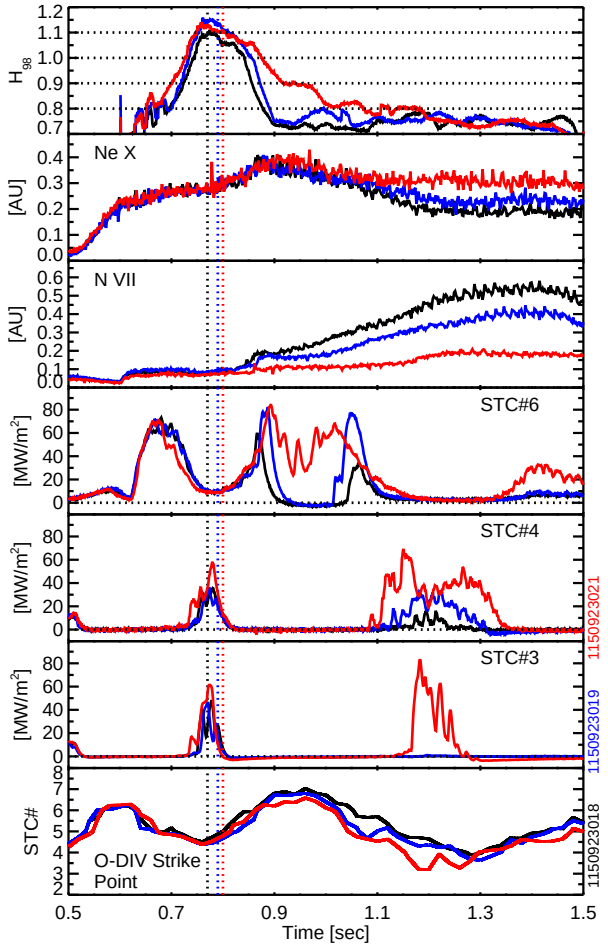

Figure 2: Core and boundary response of 1.1 MA, 5.7 T I-modes with 4.0-4.5 MW of input power with fixed pre-I-mode Ne seeding and varying intra I-mode N_2 seeding. All levels of N_2 result in I/L back-transitions, shown by H_{98}, prior to meaningful reduction of divertor heat flux, shown by STCs. Vertical dashed lines indicate when N_2 seeding first reaches the plasma.

rise in N II emission is observed, averaged over the divertor. The I/L back-transition, indicated by a vertical dotted line, occurs soon after, well before an appreciable rise in radiated power is observed (see Figure 3). This transition is identified by a step down in the $T_{e,95}$ value measured by ECE and a spike and step up in divertor D_α. The full drop of temperature occurs over a few energy confinement times as the plasma establishes a stationary L-mode. Note that only the time-evolving stored energy is plotted in Figure 3, but the pre/post transition values of H_{98} correspond to 1.05-1.10 and 0.80-0.85, respectively, while using L-mode scaling shows H_{89} changing from 1.4-1.5 to 1.0-1.1. Regardless of 0-D scaling metrics, it is clear that the thermal ETB collapses and does not rebuild after the impurity seeding. In 1160913007, estimates from the change in conductivity before ($0.8 < t < 1.0$ s) and after a stationary seeded L-mode phase is reached ($1.30 < t < 1.45$) show an increase in nitrogen concentration of 2.1±0.8%. Roughly scaling the N VII signal this implies that the pre-seeding $n_N/n_e \simeq 1\%$ and that

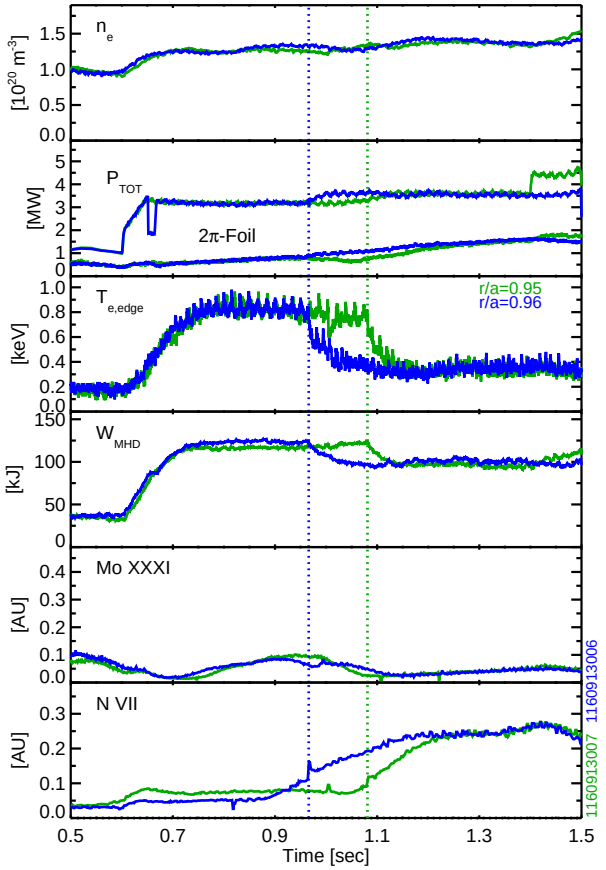

Figure 3: Comparison of two 1.0 MA, 5.4 T I-modes with no pre-I-mode Ne, but varying the timing of the intra I-mode N_2 by 150 ms, demonstrating that the I/L transition is being caused by the extrinsic seeding

the increase that triggers the I/L transition $\ll 1\%$.

At $t = 1.00$ in 1160913007 (green traces in Figure 4), there is a D_α spike and brief drop in ECE temperature. A transient far SOL rise in heat flux and SXR emission identify this as an edge localized mode (ELM), in the broader sense of the term. We note that I-modes have exhibited ELMs that are well away from Type I stability boundary [22]. While not needed to regulate the pedestal, in the context of power exhuast, I-mode ELMs necessiate further examination, including possible connection to SOL bursts seen in AUG [6], as even their infrequent occurrence could present a materials challenge in larger, high-power devices. Here, ELMs were observed occasionally in the pre-seeding phases of the I-modes and in this instance act to further demonstrate, beyond $H_{98} \geq 1.0$, that the I-modes are robust to transient changes in the edge plasma. Thus we argue the robust ELM response shows that the seeding is not simply perturbing an I-mode that is already predisposed to being pushed easily into an ETB collapse. The cause for the D_α spike is not known and is unexpected given the lack of a substantial change in the density profile from I-mode to L-mode. We note that the change in D_α is small relative to ELMs in H-mode or H/L transitions, and may be driven by the transient increase in

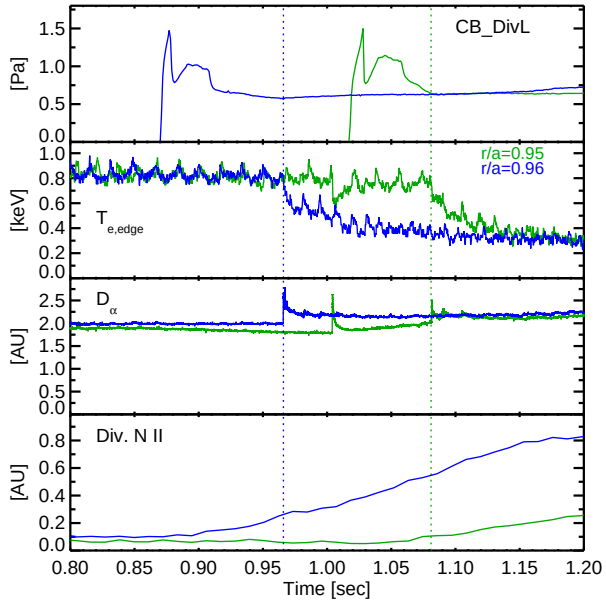

Figure 4: Further examination of the two plasmas shown in Figure 3, showing the small delay between when the gas is observed in the lower divertor between C-Port and B-Port (CB_DivL) and when the I/L transition is triggered.

power flux to PFCs due to the loss of the stored energy in the thermal ETB.

3. I/L Back-Transition Phenomenology

The inability to maintain the I-mode in the experiments summarized by Figure 2 in Section 2 led to a set of follow-up experiments to try to increase the time window between the start of seeding and I/L back-transition. The density was reduced and the RF power increased over multiple shots in an attempt to decrease the pedestal collisionality prior to seeding. The underlying hypothesis was that geodesic acoustic modes (GAMs), which are observed in the I-mode ETB [23][24], were being impacted by increased collisions, characterized by the total ion collision frequency, $\nu_i = \nu_{ii} + \nu_{iz}$, normalized to the GAM frequency, c_S/R, where c_S is the ion sound speed, $\sqrt{2T_i/m_i}$. If $\nu_i R/c_s$ becomes large, then the GAM could be broken up by collisions, and both ν_i and c_s depend on the impurity density. Note that since $q_{95} \simeq 3.5$ is held constant over this scan and c_s is smaller but close to $v_{th,i}$, trends in $\nu_i R/c_s$ are similar to edge ion collisionality, $\nu_i q_{95} R/v_{th,i}$. Time histories of relevant plasma parameters for the density scan are shown in Figure 5 while a comparison of two shots at the same density but different RF power is shown in Figure 6. The nitrogen fueling used in 1160913007 was kept fixed over all N_2 seeded plasmas, where approximately 7-8 Torr-L was injected over 450 ms, with the piezo system triggered from $0.95 < t < 1.40$. All exhibited an I/L back-transition following the nitrogen injection but with delay times varying from 30-120 ms. As shown in Figure 5, the reductions in density led to increased molybdenum in the core plasma (crimson), reducing the power crossing the separatrix. This reduces

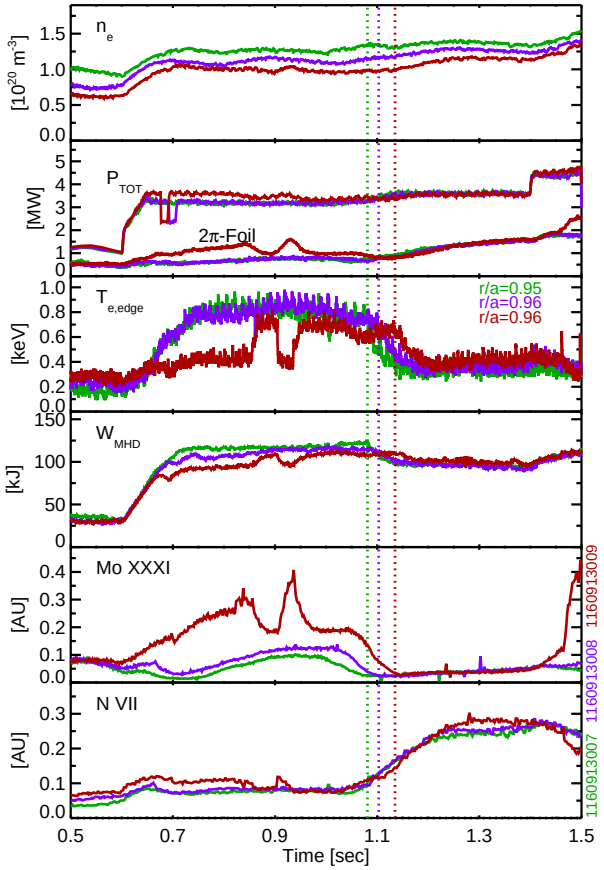

Figure 5: Density scan in 1.0 MA, 5.4 T I-modes with only intra I-mode N_2 seeding. As density is reduced, intrinsic Mo increases delaying or preveting the L/I transition but also delaying the I/L back-transition caused by seeding.

the pedestal temperature and can prevent the L/I transition. At the lowest density, an estimate of Mo concentration can be made from the on-axis, AXUV diode emissivity, as shown in [25], measured to be approximately 1.0 MW/m^3, resulting in $n_{Mo}/n_e \simeq 0.0017$, just before the first L/I transition in 1160913009. The lack of density peaking and the radial view of the VUV spectroscopy allows this concentration to be roughly scaled proportionally to the Mo XXXI VUV signal. This means that during the seeded L-mode phase, Mo concentrations are well below 10^{-3} and thus into the trace limit, and do not contribute strongly to the radiated power. Also evident is that reducing the density increased the delay from gas injection to I/L transition, but these long delays actually had larger values of $\nu_i R/c_s$, due to reduced temperature and reduced n_i/n_e, interpreted from Z_{eff} increases. This is discussed in more detail below.

The power scans were executed by increasing the ICRF power after the I-mode had been established, prior to the introduction of N_2, as shown in Figure 6. Surprisingly, despite $\simeq$1 MW higher input power, the I/L transition occurs slightly sooner at higher power (011) than in the lower power shot (007). Even later in the discharge, where the total input power has risen nearly 2 MW from the I-mode phase, the plasma remains

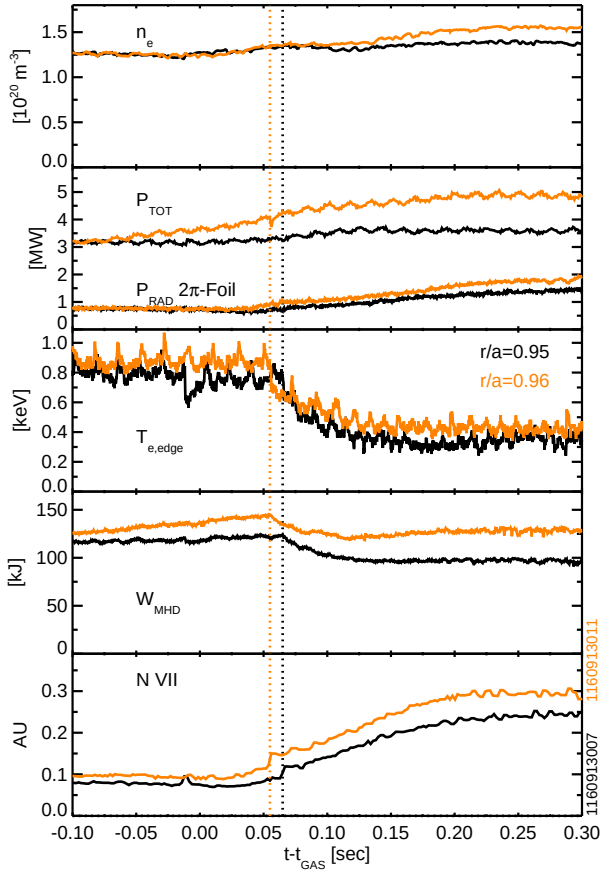

Figure 6: Comparison of two 1.0 MA, 5.4 T I-modes with only intra I-mode N_2 seeding but at varying levels of input power. Increasing P_{RF} surprisingly results in a prompter I/L back-transition and an L-mode is sustained even at higher P_{net} following seeding.

in L-mode. Even computing the power crossing the separatrix, P_{sep}, using the 2π measurement, which includes divertor radiation, P_{sep} in the L-mode is above that of the I-mode by 25-30%. This suggests the barrier to reentry into I-mode is not one of sufficient net power relative to the plasmas without seeding. Along with the limited rise in radiated power prior to the I/L back-transition, experimental results point away from excessive radiation a problem for I-mode sustainable during impurity seeding. This is further reinforced by observing that the sawtooth heat pulses during the decay of stored energy do not lead to a dithering behavior which has been noted on the L/I and the I/H transition [26].

The power and density scans led to a variation in the delay between when the pressure first rises in the divertor and when the I/L back-transition occurs. Multiple correlations were examined and those with observable trends outside of scatter are shown in Figure 7. The first two discharges in which N_2 is used are excluded. These had systematically larger delays, assumed to be due to the walls pumping the nitrogen and reducing the influx into the plasma. These results show that the best I-modes, those with the highest confinement time and pedestal pressure are those where the I/L

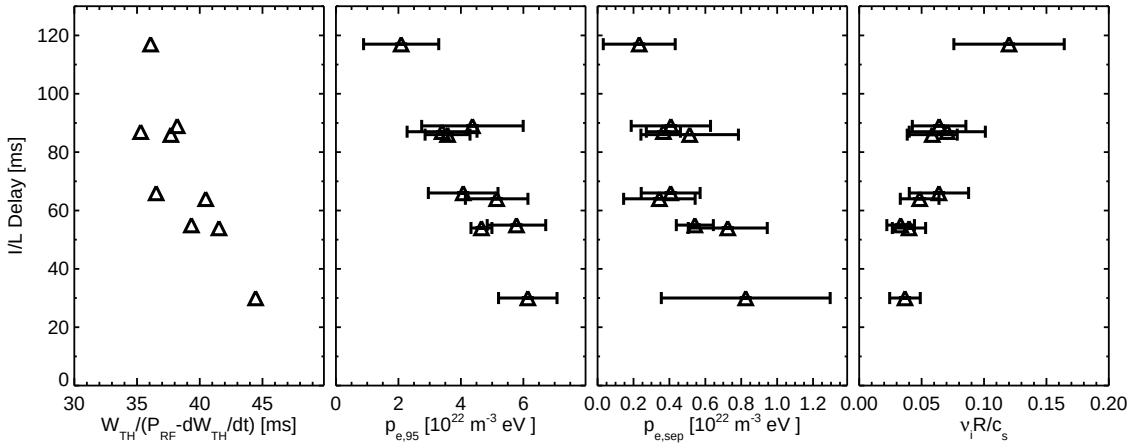

Figure 7: Correlations of the delay between injection of N_2 and the I/L back-transition with various metrics from the plasma. The longest delay is seen for the lowest performance I-mode and highest collisionality at the pedestal top.

delay is the shortest. The values for $\nu_i R/c_s$ are computed using $r/a = 0.95$ values, assuming that $T_i = T_e$ with error bars calculated by interpreting Z_{eff}, derived core visible bremsstrahlung, to be due to either Mo or N when computing n_i from n_e and the average ion mass in c_s, as well as allowing for a $\pm 15\%$ variation in T_i/T_e. This shows that plasmas with the largest $\nu_i R/c_s$ (also those with the highest ion collisionality) are those that remain in I-mode the longest following seeding. While $\nu_i R/c_s$ remains well below unity, the trend is on the opposite direction one would expect if collisions are quenching the GAM. While we should look for new explanations that are consistent with trends in Figure 7, it may also be that our measurement location is a poor indicator of where GAM damping may occur, poloidally. The GAM $m = 1$ density perturbation occurs at the top and bottom of the plasma where impurities could cause a larger change in plasma conditions local to the x-point and where high poloidal flux expansion, and thus increased parallel connection length, could create strong flux-surface integrated braking. More detailed numerical simulations would be necessary to examine if such GAM behavior could occur while also being consistent with the trends calculated here using data from outboard midplane profiles.

We have not identified a clear physics explanation for the I/L back-transition that fits these empirical trends. We cannot exclude a role for changes in mean E_r in the the I-L transition, since CXRS measurements were unavailable due to pollution of B V from N V. However, if there is such a change induced by the seeding, it must be quite subtle or localized, since pedestal T_e (equal to T_i within uncertainties) is not affected prior to the back-transition and indeed the higher $p_{e,ped}$ discharge transitioned earlier as shown in Figure 7. A wide range of C-Mod diagnostics were explored with a goal of trying to establish more evidence of causality and understand the transition physics. Figure 8 presents spectrograms from a variety of diagnostics where changes were observed between N_2 injection and the I/L transition. The Weakly Coherent Mode

(WCM) [27][23] is observed in density fluctuations near the top of the T_e pedestal using the 75 GHz reflectometry system. Changes to the WCM frequency and an increase in low frequency n_e fluctuations toward L-mode levels are observed to occur within tens of ms of the gas reaching the plasma. This expands in frequency range continuously through the I/L back-transition and is similar to a feature that is suppressed at the L/I transition as shown in prior I-mode publications [27].

Other spectrograms in Figure 8 show a mode at 15-20 kHz that is observable on large number of diagnostics measuring from the pedestal top to the outer target. The frequency is modulated by sawteeth, and in this plasma is continually present following the L/I transition, but its frequency begins to down-shift prior to the I/L back-transition. Although not shown, this mode is weak, but resolvable on the reflectometry and, time averaged, is within ± 1 kHz from the GAM frequency measured by gas puff imaging on a separate shot than the one illustrated in Figure 8. We will refer to these as GAM-frequency modes (GFM), but at this time make no claim to their being due to the GAM itself, a secondary effect or completely unrelated. Literature suggests a drop in frequency of GAMs is consistent with an increase in the impurity concentration [28], but we lack edge localized n_z measurements to make a quantitative comparison. Across our data set, a GFM is not always seen by these diagnostics when the plasma is in I-mode. Most noticeably, it is absent in the lowest density shots, but is also lost at I/L and I/H transitions. Its presence on diagnostics that observe the pedestal as well as SOL measurements like the outer-leg viewing AXUV diodes and I_{sat} fluctuations indicate a linkage between these zones. This may help explain why such a seemingly minor perturbation such as the introduction of nitrogen into the PFR can cause sufficiently widespread impact as to trigger the collapse of the thermal ETB and prevent it from being reestablished even at higher input power.

4. Seeding Impacts on Outer Divertor

In Section 2 it was shown that the I/L transition occurred before the outer target heat flux is meaningfully reduced. It will be critical to solve this problem for I-modes, but the experimental observation of substantial mitigation in the subsequent L-mode is almost equally as important. This suggests a solution may be possible, perhaps using advanced long-legged divertors [29][30], if the dissipation region can be sufficiently distinct from the I-mode pedestal as to avoid the I/L-back-transition exhibited in the current C-Mod studies. It is a necessary, but not sufficient condition that a high-power, low-density SOL can support the dissipation necessary for an I-mode edge, at least for this divertor geometry. In contrast to the H/L back-transition, the power exhaust boundary conditions across the I/L transition are relatively constant due to the lack of change in density, the continuity of power across the separatrix and the expected marginal increase in λ_q. Results in [31] indicate the heat flux width, λ_q scales as $1/\sqrt{\bar{p}}$, where $\bar{p}$ is the volume averaged plasma pressure, indicating the post-seeding L-mode in 1160913011 (orange traces in Figure 6) should have similar P_{SOL} and λ_q as the the pre-seeding lower

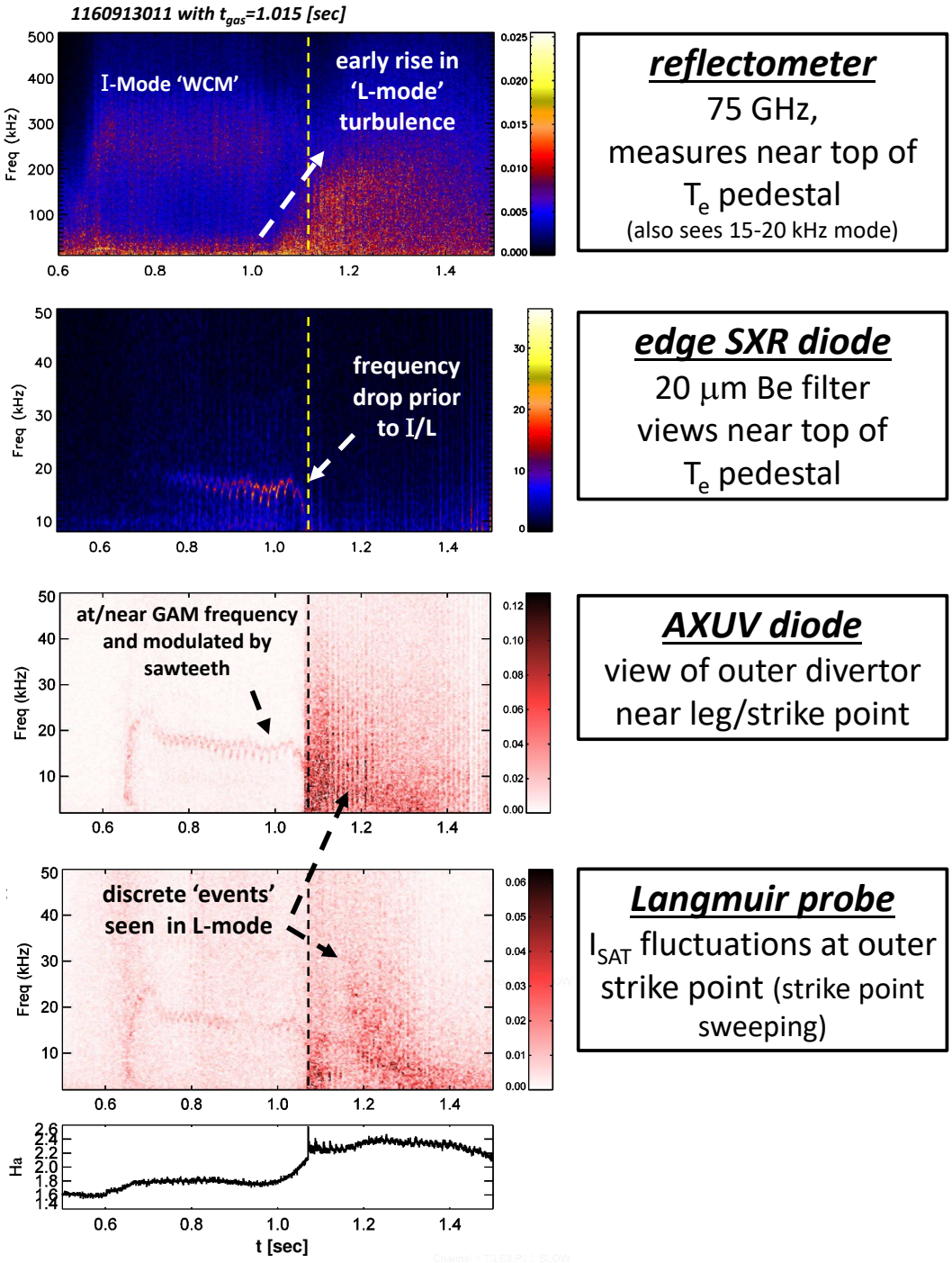

Figure 8: Time history of spectrograms from various edge and divertor diagnostics for the higher power I-mode shown in Figure 6 (orange traces). Results such as the change in the broadband density fluctuations at the pedestal top prior to the I/L transition may point to how seeding is impacting the thermal ETB.

power I-mode (black trace) as well as a similar $n_{e,sep}$, thus it should pose a similar power exhaust challenge.

The divertor response for 1160913011 is summarized in Figures 9 and 10, the former comparing spatial profiles at the outer target in the I-mode and L-mode, the latter showing time histories for pedestal and core in black, while the divertor and target conditions are shown in red. Profile positions at the target are expressed in $\rho \equiv r - r_{SEP}$, mapped to the outboard midplane. In Figures 10 and 11, probe based measurements at the outer target, T_e, $q_{\|}$ and p_e, are taken from $\rho = 0.66$ mm in the common flux region. The molybdenum source is characterized by the brightness of the 390 nm Mo I line emission, averaged over the outer divertor, while the nitrogen in the divertor is characterized using the 399.5 nm N II line, averaged over the x-point and inner divertor. The spatial profiles at the outer target, shown in Figure 9, are assembled from the spatial sweeps over the Langmuir probe arrays, compiled assuming that the floating potential, V_f, has a zero crossing at $\rho = 0$. Error bars represent the standard deviation of the measurement within the time and space bins. Significant reductions, close to an order of magnitude, in both $q_{\|}$ and T_e are observed and p_e is reduced by a factor of five at the peak. It is unknown what leads to the increase in the far private flux $q_{\|}$ and p_e, but this could be a transport effect stimulated by the impurities. An alternative explanation may be that assuming $V_f = 0$ at $\rho = 0$ for all times is wrong, and there is a shift in the L-mode profiles of nearly 2 mm into the common flux region, which leads to agreement in the far SOL pressure pre/post seeding (green curve in Figure 9). This would imply that heat flux in PFR and near-SOL are mitigated, but the far SOL is less impacted. Note that time history data in Figure 10 and 11 are plotted assuming the assumption of $V_f = 0$ at $\rho = 0$ is valid for all time windows.

Examining the time-histories presented in Figure 10, there are multiple features worth emphasizing. T_e in the divertor is shown to increase and decrease during the I-mode phase, while the p_e has a weaker variation, and is thought to be driven by the strike point sweep across the outer target and resulting variation in recycling. The reductions in target $q_{\|}$, T_e and p_e happen on a slower time-scale than the pedestal T_e which reflects the I/L back-transition. The time evolution of plasma parameters at the target follows more closely the increase of N II emission. The seeding also shows the divertor Mo emission is driven down to effectively zero. The core Mo level, which also has a main-chamber ICRF-driven component, is relatively de-coupled from the dynamics of the outer-target Mo emission, consistent with historical observations of compression using the vertical plate divertor [32]. While the starting conditions can vary across different points in the density and power scans presented earlier, the final conditions are relatively similar. The Mo I emission is eliminated, the target temperature clamps to $\simeq$5 eV and $q_{\|}$ drops to below 50 MW/m^2. The amount of impurities injected remain fixed, but the N II line emission increases. For example, between shots 1160913007 and 011, shown in Figure 6, the change in N II emission increases by a factor of three, while the change in core N VII is relatively fixed. Thus it seems that sufficient nitrogen is accessible to the divertor plasma for it to respond to increases in $q_{\|}$ by enhancing radiation, to drive the plasma to the same equilibrium condition.

In these plasmas, the response to nitrogen seeding is much better diagnosed for the

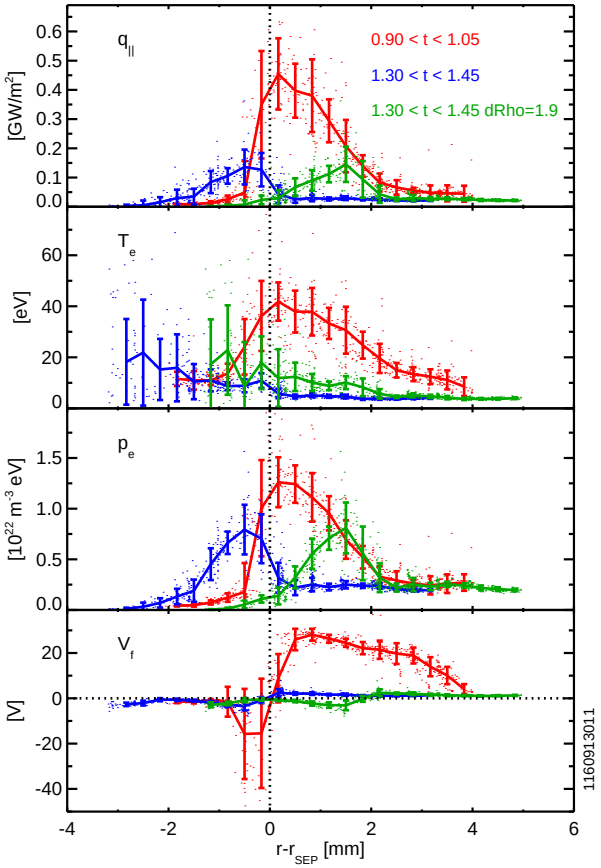

Figure 9: Comparison of plasma parameters measure by Langmuir probes mounted in the outer target prior (red) and after seeding where two methods are used to align the profiles obtained during strike point sweeping. One method (blue with red) assumes the $V_f = 0$ occurs at the same $r - r_{SEP}$, assumed here to be $r - r_{SEP} = 0$, while the other (green with red) matches the electron pressure in the far SOL.

outer divertor. It is important to note that with reversed $B \times \nabla B$, the power flux to the inner target may be slightly higher than the outer and present a larger detachment challenge. Inner target probe measurements available in the pre-seeding I-mode confirm similar $q_{\|}$ and T_e as the outer, and spectroscopic measurements show the Mo source is also eliminated. Unfortunately, the strike point scan during the seeding phase moves the inner target over probes which were non-functional during these experiments, so there is no post-seeding data. Further investigation of inner divertor conditions in dissipative I-modes (or high power, low-density L-modes) is necessary.

Figure 11 shows the same time histories as Figure 10 but for the plasma with the largest amount of main-chamber neon seeding and no divertor nitrogen seeding, confirmed by N II signals that remain less than approximately one third of the pre-N_2 seeding level of earlier shots. A 150 ms Ne puff, starting at 0.95 seconds, injects approximately 0.25 Torr-L into the main-chamber, and its recycling behavior enables a stationary level to be reached in the plasma. This is nearly twice the amount injection

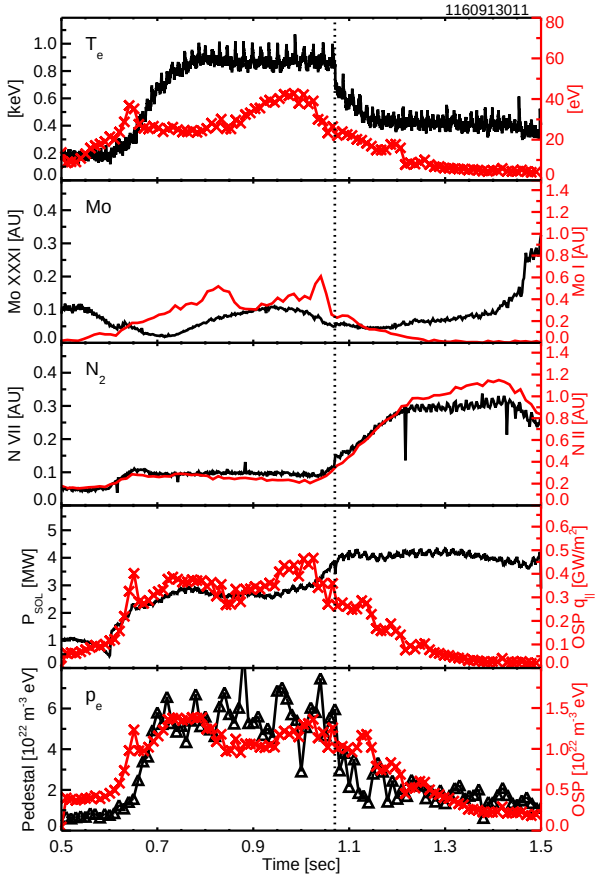

Figure 10: Time evolution of the core/pedestal parameters (black) and outer target conditions/divertor conditions at $r - r_{sep} = 0.66$ mm (red) for intra I-mode N_2 seeding showing the gradual but large drop in T_e, $q_{\|}$ at the outer target.

into I-modes such as 1120907028 (0.12 Torr-L) or that used for the recycling gas in discharges discussed in Figure 2. The reduction in pedestal T_e measured by ECE occurs much later following the rise of core Ne from VUV spectroscopy and drops more gradually over approximately 100 ms. The sharp D_α feature at the I/L back-transition is not seen as in the nitrogen plasmas. Still, the SXR fluctuations show a loss of the GFM at $t \simeq 1.1$ s, and the reflectometer shows a similar loss of the WCM and rise in low-frequency fluctuations concurrent with the beginning of the drop in pedestal T_e. This behavior is more in line with less abrupt I/L transitions observed as net power is reduced, either by dropping P_{ICRF} or due to increasing P_{RAD} from rising Mo. The same L-mode upstream conditions are obtained, but the outer-target temperature and parallel heat flux are much higher, with T_e bottoming out near 15 eV and showing large amplitude increases following sawteeth. This is consistent with the inability to eliminate the Mo I emission, which itself shows an aliased oscillatory feature. A comparison of the divertor target profiles following Ne and N_2 seeding is shown in Figure 12, for matched pre-seeding target conditions. Note that the error bars for the Ne seeding case near the strike point appear to be due to the variations between two plasma states driven

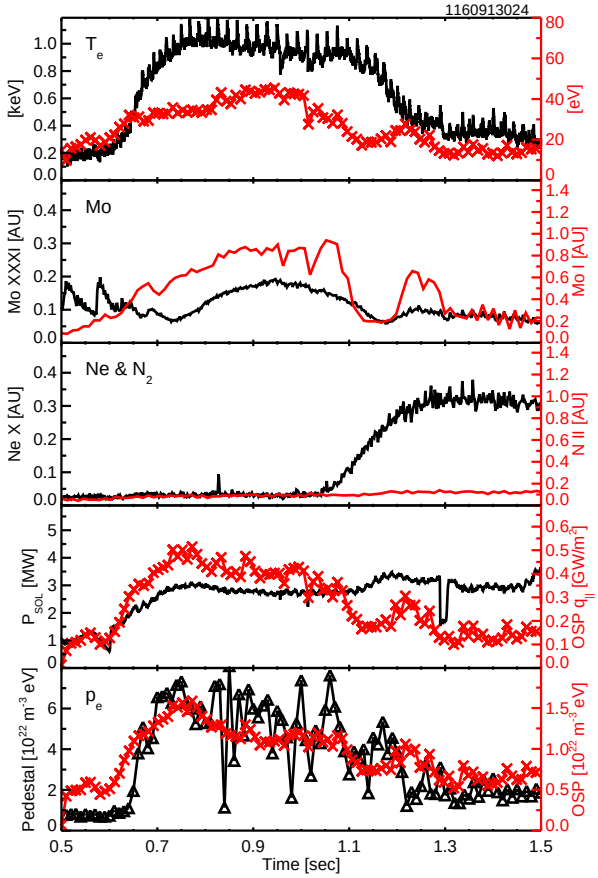

Figure 11: Time evolution of the core/pedestal parameters (black) and outer target conditions/divertor conditions at $r - r_{sep} = 0.66$ mm (red) for intra I-mode Ne seeding showing the gradual but more limited drop in T_e, $q_{\|}$ relative to Figure 10.

by sawteeth, not random error. A repeated plasma with 55-65% as much Ne injected was able to maintain an I-mode ETB and sustain the WCM along with a factor of two reduction T_e and $q_{\|}$ from the I-mode targets. This makes contact with prior I-mode operations where weak Ne seeding is compatible with I-mode, and shows that Ne-based detachment is both incompatible with I-mode and was also not achievable within our scans in high power, low-density L-mode. Note that when comparing the post-seeding L-modes between Ne and N_2, the neon seeded plasma resulted in a 40% increase in line-averaged density. Closer inspection revealed the Ne seeding resulted in peaking of the density profile at a nominally fixed separatrix density, and was present, although weaker, in Ne-seeded plasmas that remain in I-mode. Ne seeding resulted in elevated D-D neutron rates compared to the N_2 reference indicating the peaking was in main-ions and not impurities.

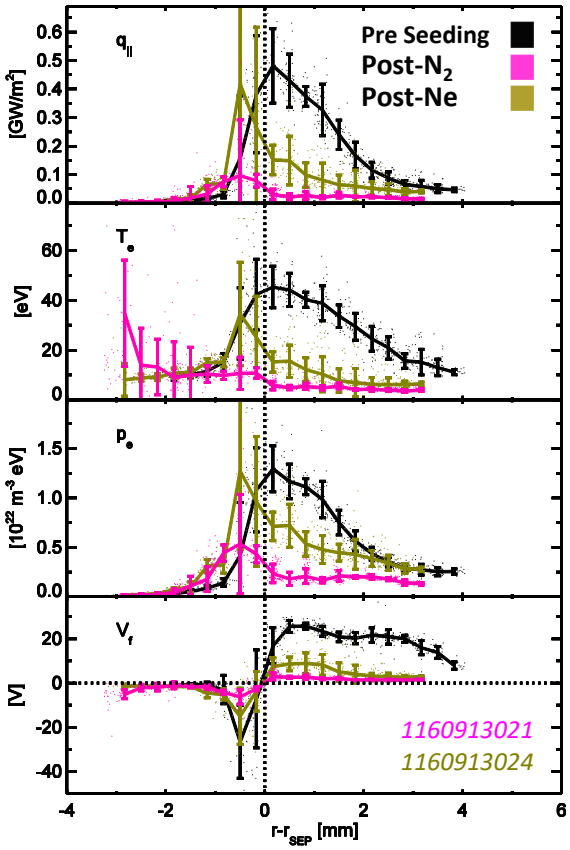

Figure 12: Comparison outer divertor profiles prior (black) and after seeding using N_2 (magenta) and Ne (brown) for matched target plasmas. This assumes the $V_f = 0$ occurs at $r - r_{SEP} = 0$.

5. Summary and Discussion

As shown above for a series of experiments on Alcator C-Mod, no integrated dissipative divertor scenario with a high core energy confinement, $H_{98} > 1$ was found in the I-mode regime. The I-mode transitioned back to L-mode in which dissipation was substantial when using private flux N_2 seeding. No issue with discharge stability (e.g. MARFE-induced disruptions) was encountered over a range of densities and input powers. Achievement and control of full detachment in the L-mode was not directly pursued but was thought to be achieved in a single case where nitrogen seeding resulted in large amplitude ($\simeq$20%), low frequency (20-30 Hz) line-averaged density oscillations, characteristic of full poloidal detachment. The L-mode results are important in demonstrating that high $q_{\|}$, low density SOL plasmas can still sustain a large amount of dissipation using low-Z impurities. It would be useful to explore these discharges further with fluid modeling codes to see if such tools properly capture the radiating efficiency of the low-Z impurity, helping to validate the physics which is approximated in simple models by varying $n_e\tau$ [33]. This could also include attempts to simulate

the differences between nitrogen and neon seeding which were particularly striking experimentally.

The sensitivity and promptness of the I/L transition with extrinsic N_2 but not Ne is confusing given the variation in typical intrinsic impurities observed in prior C-Mod I-modes: boron due to boronization, oxygen from overheating boron coated limiter tiles and fluorine from overheating polytetrafluoroethylene (PTFE - i.e. teflon) used in-vacuum. If the I-mode regime is sensitive to small concentrations of low-Z impurities, as shown by extrinsic N_2 seeding, it would seem to preclude the establishment of the wide operational space C-Mod has shown. Instead I-mode operational space would be hyper-sensitive to the evolution of wall conditions and contamination. As mentioned earlier, a robust I-mode like 1120907028 [7] had extrinsic neon seeding, but an increase of intrinsic oxygen was also observed, thought to be from fast-ion heating of the main-chamber limiter, yet that discharge is an example of a high-performance I-mode. This suggests that the type of impurity and perhaps the injection location may be important such that private flux N_2 is specifically problematic, and raises the possibility of surface chemistry playing a role. When nitrogen is seeded into plasmas where PFCs are saturated, recycling of ammonia into the plasma may occur, resulting in an effective private flux region injection of deuterium that we are not considering. The longer delay between start of N_2 seeding and the I/L transition during the first seeding discharges of the day support the idea that recycled and not prompt N_2 seeding may be important. Still, on all shots where an I/L transition was induced by N_2, an I-mode was established in the subsequent plasma, except in cases of elevated Mo, despite noticeable levels of residual divertor N II and main-chamber N VII emission prior to seeding, as shown in Figure 10. Comparing 1160913007, shown in Figure 3, with a repeat after seven N_2 seeded plasmas, the I-mode was established despite residual nitrogen being over twice as high, as indicated by relative N VII brightness.

Of almost equal importance is the manner in which these plasmas responded to the low-Z seeding. While the triggering of an H/L back-transition through excessive impurity seeding has been reported on multiple devices [20] [34], the I/L transitions reported here do not appear to be connected to increased radiation in the confined plasma which could starve the pedestal of the power it needs to sustain the ETB, as was inferred for Ar on C-Mod [35]. Nor do the C-Mod I-modes studied here appear to enter a low-frequency 'dithering' type of behavior as has seen on JET [36]. The results reported in Section 7 investigating the spectrograms of multiple diagnostics, while not exhaustive, represent a thorough description of the plasma behavior. At this time, there does not appear to be a physics picture that explains the evolution of the pedestal response following N_2 seeding. Unlike the L-mode exhaust results which should be modeled by standard fluid modeling tools, the pedestal physics requires simulation tools that can explore smaller spatial structures and look at self-consistent turbulence evolution. It may be useful to apply tools such as XGCa [37], Hermes [38] or GRILLIX [39] to the C-Mod I-mode plasmas to narrow the range of physical mechanisms that might be at work, although code enhancements may be needed to capture the impacts of

non-trace impurities. Further experimental investigations would benefit from modeling being able to suggest physical mechanisms for the sensitivity to impurities and possible observables. For example, if GAM quenching localized to the x-point is important, how can this be measured within limited diagnostic sets?

Both of these results would benefit from further study, but additional experiments are no longer possible on Alcator C-Mod. Other devices have demonstrated I-mode operation, but at lower field where the window between L/I/H is rather small [7]. Despite this, tokamaks that have explored I-mode (e.g. DIII-D, AUG) should be able to confirm if the C-Mod results of extreme sensitivity to low-levels of N_2 are replicated. If observed, further study of the pedestal physics is possible.. Measurements of E_r evolution across the L-I and I-L transitions should be feasible and would help clarify the role of mean radial electric field shear in the transitions and transport changes. If new experiments show I-mode radiative exhaust phenomenology to be closer to H-mode, in which the primary consideration is maintaining net power through the pedestal, there will still be a need for more I-mode capable tokamaks. It may be difficult in AUG and DIII-D to study radiative exhaust in plasmas where the power margin between the confinement transition is rather small, since in conventional divertors, impurity-based exhaust schemes typically result in a modest increase in core radiation to substantially increase radiation in the SOL/divertor. This further emphasizes the need for existing higher field devices such as KSTAR, WEST and JET to explore I-mode, and should motivate considerations of I-mode scenarios on the proposed Italian DTT [40] and Compass Upgrade [41] tokamaks. The near-term replication of the C-Mod experiments is very important for the consideration of I-mode as a reactor scenario, as we need to understand if the sensitivity to seeding is characteristic of the closed, short-legged vertical plate divertor. If so, then advanced, long-legged divertors need to be explored for I-mode. This underscores the need for a new high-field, high-power-density divertor test tokamak, such as the proposed ADX facility [42].

6. Acknowledgments

This work is supported in part by US Department of Energy award DE-AC05-00OR22725 and DE-SC0014264, using Alcator C-Mod, a DOE Office of Science User Facility. The authors would like to thank the diligent and dedicated Alcator C-Mod operational staff for expert operation of the tokamak during the 2015-2016 campaigns when these experiments were conducted.

7. References

[1] A. Loarte R. Neu. *Fusion Eng. Design*, 122:256, 2017.
[2] F. Ryter, *et al*. In *Proc. of the 22nd EPS Conference on Controlled Fusion and Plasma Physics*, pages 89–92.
[3] D. Whyte, *et al*. *Nucl. Fusion*, 50:105005, 2010.
[4] A. Marinoni, *et al*. *Nucl. Fusion*, 55:093019, 2015.

[5] F. Ryter, *et al*. *Nucl. Fusion*, 57:016004, 2017.
[6] T. Happel, *et al*. *Plasma Phys. Control. Fusion*, 59:014004, 2017.
[7] A. Hubbard, *et al*. *Nucl. Fusion*, 56:086003, 2016.
[8] A. Hubbard, *et al*. *Nucl. Fusion*, 57:126039, 2017.
[9] A. Loarte, *et al*. *Phys. Plasmas*, 18:056105, 2011.
[10] J.W. Hughes, *et al*. *Nucl. Fusion*, 51:083007, 2011.
[11] M. Greenwald, *et al*. *Phys. Plasmas*, 21:110501, 2014.
[12] D. Brunner, *et al*. *Nucl. Fusion*, 57:086030, 2017.
[13] A. Kuang, *et al*. *Rev. Sci. Instrum.*, 89:043512, 2018.
[14] D. Brunner, *et al*. *Rev. Sci. Instrum.*, 83:033501, 2012.
[15] N. Basse, *et al*. *Fusion Sci. Tech.*, 51:476, 2007.
[16] M.L. Reinke, *et al*. *Rev. Sci. Instrum.*, 81:10D736, 2010.
[17] Y. Lin, *et al*. *Rev. Sci. Instrum.*, 70:1078, 1999.
[18] J.L. Terry, *et al*. *J. Nucl. Mater*, 390-391:339, 2009.
[19] T.S. Pedersen, *et al*. *Rev. Sci. Instrum.*, 70:586, 1999.
[20] M.L. Reinke, *et al*. *Plasma Phys. Control. Fusion*, 59:122002, 2017.
[21] J. Lore, *et al*. *Phys. Plasmas.*, 22:056106, 2015.
[22] J.R. Walk, *et al*. *Phys. Plasmas.*, 21:056103, 2014.
[23] I. Cziegler, *et al*. *Phys. Plasmas.*, 20:055904, 2013.
[24] I. Cziegler, *et al*. *Phys. Rev. Letter.*, 118:105003, 2017.
[25] L. Delgado-Aparicio, *et al*. *Rev. Sci. Instrum.*, 83:10E517, 2012.
[26] A. Hubbard, *et al*. *Nucl. Fusion*, 52:114009, 2012.
[27] A. White, *et al*. *Phys. Plasmas*, 51:113005, 2011.
[28] W. Guo, *et al*. *Phys. Plasmas*, 17:112510, 2010.
[29] P.M. Valanju *et al*. *Phys. Plasmas*, 16:056110, 2009.
[30] M. Umansky, *et al*. *Phys. Plasmas*, 24:056112, 2017.
[31] D. Brunner, *et al*. *Nucl. Fusion*, 58:094002, 2018.
[32] B. Lipschultz *et al*. *Nucl. Fusion*, 41:585, 2001.
[33] A. Kallenbach, *et al*. *Plasma Phys. Control. Fusion*, 55:124041, 2013.
[34] M. Bernert, *et al*. *Nuc. Mater. Energy*, 12:111, 2017.
[35] M.L. Reinke, *et al*. *J. Nucl. Mater*, 415:S340, 2011.
[36] A. Huber, *et al*. Impact of strong impurity seeding on the radiation losses in jet with iter-like wall. In *Proc. of the 41st EPS Conference on Controlled Fusion and Plasma Physics*.
[37] R. Hagar, C.S. Chang. *Phys. Plasmas*, 23:042503, 2016.
[38] B.D. Dudson J. Leddy. *Plasma Phys. Control. Fusion*, 59:054010, 2017.
[39] A. Stegmeir *et al*. *Plasma Phys. Control. Fusion*, 60:035005, 2018.
[40] R. Albanese *et al*. *Nucl. Fusion*, 57:016010, 2017.
[41] R. Panek, *et al*. *Fusion Eng. Design*, 123:11, 2017.
[42] B. LaBombard, *et al*. *Nucl. Fusion*, 55:053020, 2015.